J Mol Model (2013) 19:4909–4917
DOI 10.1007/s00894-013-1988-4

ORIGINAL PAPER

Easy methods to study the smart energetic TNT/CL-20 co-crystal

Huarong Li · Yuanjie Shu · Shijie Gao · Ling Chen · Qing Ma · Xuehai Ju

Received: 23 June 2013 / Accepted: 27 August 2013 / Published online: 17 September 2013

Abstract 2,4,6,8,10,12-hexanitro-2,4,6,8,10,12-hexaazaiso-wurtzitane (CL-20) is a high-energy nitramine explosive with high mechanical sensitivity. 2,4,6-trinitrotoluene (TNT) is insensitive but by no means a high performance explosive. To reveal the significant importance and smart-material functionality of the energetic-energetic co-crystals, the stability, mechanical and explosive properties TNT/CL-20 co-crystal, TNT crystal and CL-20 crystal were studied. Non-hydrogen bonded non-covalent interactions govern the structures of energetic-energetic co-crystals. However, it is very difficult to accurately calculate the non-covalent intermolecular interaction energies. In this paper, the local conformation and the intricate non-covalent interactions were effectively mapped and analyzed from the electron density (ρ) and its derivatives. The results show that the two components TNT and CL-20 are connected mainly by nitro–aromatic interactions, and nitro–nitro interactions. The steric interactions in TNT/CL-20 could not be confronted with the attractive interactions. Moreover, the scatter graph of TNT crystal reveals the reason why TNT is brittle. The detailed electrostatic potential analysis predicted that the detonation velocities (*D*) and impact sensitivity for the compounds both increase in the sequence of CL-20 > TNT/CL-20 co-crystal > TNT. Additionally, TNT/CL-20 co-crystal has better malleability than its pure components. This demonstrates the capacity and the feasibility of realizing explosive smart materials by co-crystallization, even if strong hydrogen bonding schemes are generally lacking in energetic materials.

Keywords Smart explosive · Intermolecular interaction · TNT/CL-20 co-crystal · Structure and properties

H. Li · Y. Shu (✉) · L. Chen · Q. Ma
Institute of Chemical Materials, China Academy of Engineering Physics, Mianyang 621900, China
e-mail: 215699921@qq.com

H. Li · Q. Ma · X. Ju
Department of Chemistry, Nanjing University of Science and Technology, Nanjing 210094, China

S. Gao
TCM Comprehensive Experiment Teaching Center, Shandong University of Chinese Medicine, Shandong 250355, China

Introduction

Because of their inherent safety-power contradiction [1], energetic materials are based on a very small number of compounds. "Energetic co-crystals", built up of two or more neutral molecules that are solid at ambient conditions in their pure forms [2–5], are of great interest to scientists. Such compounds not only exhibit intermediates for the production of new polymorphs but also possess some distinctly improved properties relative to pure components alone [6–8]. Much of the existing literature on co-crystal formation focuses on the exploitation of classical hydrogen bonding schemes [9, 10]. However, these hydrogen bonding schemes and the information on supramolecular synthons suitable for energetics are generally lacking in energetic materials. Consequently, the rational design of energetic co-crystals is hindered.

Recently, Landenberger [11, 12] modified the properties of 2,4,6-trinitrotoluene (TNT) and 1,3,5,7- tetranitro-1,3,5,7-tetrazacyclooctane (HMX) via co-crystallization. They also noted that the relationship of density to detonation properties no longer applies when co-crystallizing an energetic material with a non-energetic material. Even though the overall density (TNT/1-bromonaphthalene co-crystal, 1.737 g/cm^3) is greater than that of monoclinic TNT (1.713 g/cm^3), the effective density of TNT is reduced to 0.909 g/cm^3, diluting the TNT. In this case, Bolton [13] prepared an energetic–energetic co-crystal composed of 2,4,6,8,10,12-hexanitro-2,4,6,8,10,12-

hexaazaisowurtzitane (CL-20) and TNT with a 1:1 molar ratio, which combines the economy and stability of TNT with the density and power of CL-20 to create a homogenous energetic with high explosive power and excellent insensitivity (Fig. 1). Stimulated by the results of the CL-20/TNT co-crystal, more and more scientists have focused their interest on the development of energetic–energetic co-crystals from the nitro-rich, non-aromatic compounds that dominate the field with great confidence [14–18].

However, there is still no reliable set of rules that would allow us to predict formation, stoichiometry, and structure of an energetic co-crystal. So we are still far from a deep understanding of the formation processes of crystals [19]. On the other hand, an understanding of the resulting structures seems to be an achievable goal by theoretical methods, in particular for identifying the intricate non-covalent interactions that govern the structures and properties of co-crystals. A co-crystal can be constructed through several types of interaction, including hydrogen bonding, π–π stacking interactions and van der Waals (vdWs) forces [20–22].

In the energetic materials field, the atomic interaction lines (AILs) or radius distribution function (RDF) usually utilized to study hydrogen bonding can indicate only the probable existence and strength of hydrogen bonds and vdWs forces. The best way to reveal these intermolecular interaction forces is by calculating intermolecular interaction energies. However, the accurate calculation of intermolecular interaction energies, especially vdWs forces, is difficult with existing methods. In recent years in the field of pharmaceutics, charge density analysis based on experimental and theoretical calculations has reached the stage where topological features allow net atomic charges and related one-electron properties to be obtained, leading directly to the derivation of features related to chemical bonding [23]. In 2010, Erin [24] presented an approach to map and analyze non-covalent interactions in small molecules, molecular complexes and solids, requiring only molecular geometry information. This technology provides us with an approach to understand more about energetic co-crystals.

In this paper, theoretical calculations were used to investigate the properties and nature of intermolecular interactions in TNT/CL-20 co-crystal. Quantum mechanical/molecular dynamics methods were employed to probe the stability, and mechanical and explosive properties, of TNT/CL-20 co-crystal. On the basis of electron density and its derivatives, intricate non-covalent interactions, such as vdWs interactions, hydrogen bonds (HBs) and steric repulsion stacking (SRs) interactions, were detected, distinguished and highlighted in TNT/CL-20 co-crystal.

Computational methods

Structure calculations

The density functional theory (DFT) quantum mechanical code, DMol^3, was used to optimize the structures of molecules and crystals of the TNT/CL-20 co-crystal system. Since it can quickly and efficiently perform structure optimizations of molecular or some crystal systems using delocalized internal coordinates [25–29]. The exchange-correlation interaction was treated by functional Perdew, Burke and Ernzerh of generalized gradient approximation (PBE-TS GGA) [30], and the applied basis set was a double numerical basis set plus d-functions (DND). Dispersion-corrected functional (DFT-D) based on an additive pairwise summation of dispersion energy contributions between all pairs of atoms in the system to the total energy was employed to exactly calculate the weak vdWs forces [21–36]. A convergence criterion of 10^{-6} a.u. on the total energy was used in self-consistent field (SCF) calculations. The global orbital cutoff was taken to be 400 pm. The generated structure was minimized using the convergence threshold. The value of the maximum energy change is 1×10^{-5} Hartree. The maximum force and maximum displacement is 0.02 Hartree nm^{-1} and 0.05 nm, respectively. The core treatment parameter was described by the all electron method.

Detection of weak interaction regions

A major problem with DFT is extraction of accurate energy for dispersion, which is the main composition of vdWs forces.

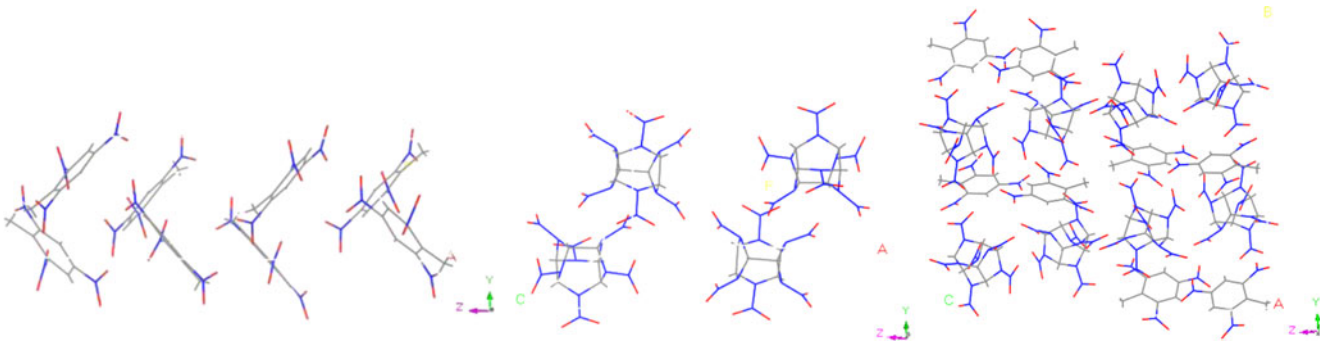

Fig. 1 Crystal structures of 2,4,6-trinitrotoluene (TNT) (*left*), CL-20 (*middle*) and TNT/CL-20 (2,4,6,8,10,12-hexanitro-2,4,6,8,10,12-hexaazaisowurtzitane) co-crystal (*right*)

The theory of atoms in molecules (AIM) has been used to understand and quantify weak interactions based on electron density [ρ(r), Eq. 1] since 1999 [37]. This approach relies on the fact that bond critical points (BCPs) of the electron density, where the gradient norm of electron density [$\nabla\rho$(r), Eq. 2] is zero, arise when atoms interact. If the interaction is bonding, the point is expected to be a first order saddle point.

$$\rho(r) = \sum_i \eta_i |\varphi_i(r)|^2 = \sum_i \eta_i \left| \sum_l C_{l,i}\chi_l(r) \right|^2 \quad (1)$$

$$|\nabla\rho(r)| = \sqrt{\left(\frac{\partial\rho(r)}{\partial x}\right)^2 \sqrt{\left(\frac{\partial\rho(r)}{\partial y}\right)^2} \sqrt{\left(\frac{\partial\rho(r)}{\partial z}\right)^2}} \quad (2)$$

Electron density ρ(r) (Eq. 1) has been found to correlate with interaction energy in hydrogen bond (HB) complexes [38, 39]. It is difficult to establish a correlation between the value of ρ at a BCP and the binding energy of no-bonding vdWs systems. Reduced density gradient (RDG, Eq. 3) can be used to highlight weak interaction regions. RDG is a fundamental dimensionless quantity in DFT used to describe the deviation from a homogeneous electron distribution [40–43]. In Bader's AIM theory [12], ρ(r) is aggregated at (3, −1) critical point (CP), which appears in the chemical bond path or between the atoms and indicates attractive interaction, while ρ(r) is depleted at (3, +1) CP, which generally appears in the center of a ring system and displays a steric effect (also called nonbond overlap). On the basis of the above conception, to reveal weak interaction regions, Erin et al. [44] developed the non-covalent interactions (NCI) index based on the relationship of functions RDG and Ω(r) (Eq. 4):

$$\mathrm{RDG}(r) = \frac{1}{2(3\pi^2)^{1/3}} \frac{|\nabla\rho(r)|}{\rho(r)^{4/3}} \quad (3)$$

$$\Omega(r) = \mathrm{Sign}(\lambda_2(r))\ \rho(r) \quad (4)$$

where η_i is the occupation number of orbital i, χ is the basis function. C is the coefficient matrix, and the element of ith row jth column corresponds to the expansion coefficient of orbital j with respect to basis function i. Sign[$\lambda_2(r)$] means the sign of the second largest eigenvalue of electron density Hessian matrix at position r.

Mechanical properties

On the basis of an optional re-optimization of the structure, mechanical properties were estimated using the "constant strain" approach [32]. In elastic mechanics, the generalized Hooke's laws can be written as follows [45]:

$$\begin{bmatrix} \sigma_x \\ \sigma_y \\ \sigma_z \\ \sigma_{yz} \\ \sigma_{xz} \\ \sigma_{xy} \end{bmatrix} = \begin{bmatrix} C_{11} & C_{12} & C_{13} & C_{14} & C_{15} & C_{16} \\ C_{21} & C_{22} & C_{23} & C_{24} & C_{25} & C_{26} \\ C_{31} & C_{32} & C_{33} & C_{34} & C_{35} & C_{36} \\ C_{41} & C_{42} & C_{43} & C_{44} & C_{45} & C_{46} \\ C_{51} & C_{52} & C_{53} & C_{54} & C_{55} & C_{56} \\ C_{61} & C_{62} & C_{63} & C_{64} & C_{65} & C_{66} \end{bmatrix} \quad (5)$$

Although the elastic coefficient matrix of an extremely anisotropic body should satisfy the formula: $C_{ij} = C_{ji}$, there are at most 21 independent elastic coefficients because of the existence of strain energy. In addition, the number of independent elastic coefficients decreases as the geometrical symmetry increases. All the mechanics properties generally can be evaluated by the elastic coefficient matrix. The Young's modulus (E), Poisson's ratio (γ), bulk modulus (K) and shear modulus (G) may be written in terms of the Lame' coefficients (λ and μ) as follows [46]:

$$E = \frac{\mu(3\lambda + 2\mu)}{\lambda + \mu}, \gamma = \frac{\lambda}{2(\lambda + \mu)}, G = \mu, K = \lambda + \frac{2}{3\mu} \quad (6)$$

For an isotropic substance, there are only two independent elastic coefficients C_{11} and C_{12} ($C_{11} - C_{12} = 2\ \mu$ and $C_{12} = \lambda$). Assuming a material as isotropic, the program can calculate the effective isotropic mechanical properties. Accordingly, each modulus and Poisson's ratio can be revealed [47], which can be estimated by loading experiments of molecular dynamics (MD) simulations in Materials Studio 6.0 (MS 6.0). The MD simulation boxes contain 4×4×4 crystallographic unit cells.

Molecular dynamics simulation

Performed by classical mechanics, a MD simulation is a computer simulation technique where the time evolution of a set of interacting atoms is followed by integrating their equations of motion. One strength of the MD method with respect to other methods such as molecular mechanics (MM) is that the time evolution of properties of the system is followed, and information on the dynamics of the system is fully presented [48]. In this work, we used MD simulations to evaluate the elastic coefficients of TNT/CL-20 co-crystal. Minimized structures with global energy minimum serve as starting basis for MD calculations. Thus, the lattice parameters and atomic coordinates were first minimized to identify the geometry of the system that corresponds to minimum points of the energy surface. Basing on the optimized structures, MD simulations were performed in an NPT ensemble (constant number of molecules, pressure, and temperature) using the forcite

module. Periodic boundary conditions were enforced by creating images of the atoms in the primary simulation cell [49]. The MD simulation boxes contain 4×4×4 crystallographic unit cells for the pure TNT, CL-20 crystal and TNT/CL-20 co-crystal. These choices of the simulation boxes ensure the use of a cutoff distance for the intermolecular potentials of about 12.5 Å. The systems were then equilibrated at 298 K and atmospheric pressure. The systems were first integrated for 1.6×10^5 time steps to reach the mechanical and thermal equilibrium for this system, and then for the production runs of 4×10^4 time steps, during which data were collected for subsequent analysis. A fixed time step size of 1 fs was used in all cases [16]. An Anderson thermostat [50] was used to control the system. For potential energy calculations, long range Coulombic and vdW interactions were evaluated using Ewald's method [51, 52] with COMPASS force field [53]. All MD and calculations of crystal structures were performed on the commercial molecular modeling software package MS 6.0 [54].

Results and discussion

Molecular geometries

In this paper, we utilized the DMol^3 program to study structures interrelated with the TNT/CL-20 co-crystal, including TNT dimer, CL-20 dimer and 1:1 TNT/CL-20 supermolecule, TNT crystal, CL-20 crystal and TNT/CL-20 co-crystal. Here, it should be noted that letters **a** and **b** stand for two kinds TNT dimer. Accordingly, the letters **c** and **d** represent CL-20 dimer and TNT/CL-20 dimer, respectively.

Atomic interaction lines (AILs) are used to describe the paths of maximum electron density [55]. First of all, we utilized AILs in the intermolecular region to denote the dominant atom–atom interactions underlying the vdW interactions. It should be noted that we considered the length of vdW AILs to be not more than 0.3 nm. Figure 2 show that the two AILs between TNT dimer **a** are shorter than that of dimer **b**, which indicates that the intermolecular interaction between dimer **a** is stronger than that of **b**. Similarly, it can be estimated that the strength of intermolecular interaction of the four compounds in Fig. 2 decreases in the order: **c** > **a** > **d** > **b**.

Table 1 lists the energetic data of the molecules, including DFT-D correction (E_C), total DFT-D energy (E_{TOT}), intermolecular interaction (ΔE_{II}). The $\Delta E_{II}<0$ of **d** in Table 1 predicts that the reaction TNT crystal + CL-20 → TNT/CL-20 co-crystal is spontaneous. More importantly, the strength of the intermolecular interaction of the four compounds in this case decreases in the order: **d** > **c** > **a** > **b**, which does not agree with the above AIL result. Here, we conclude that vdWs are not the only interactions maintaining the stability of TNT, CL-20 crystals and TNT/CL-20 co-crystal. Moreover, the CL-20/TNT dimer has the largest ΔE_{II} of the supermolecules in Table 1, which indicates that a TNT molecule and a CL-20 molecule can indeed form a new stable structure.

Electrostatic potential

Electrostatic potential (ESP) is the net electrostatic effect from the total molecular charge distribution (nuclei plus electrons). As being physical observable, the results obtained from ESPs are usually realistic. In some cases, $V_{MEP}(r)$ allows the

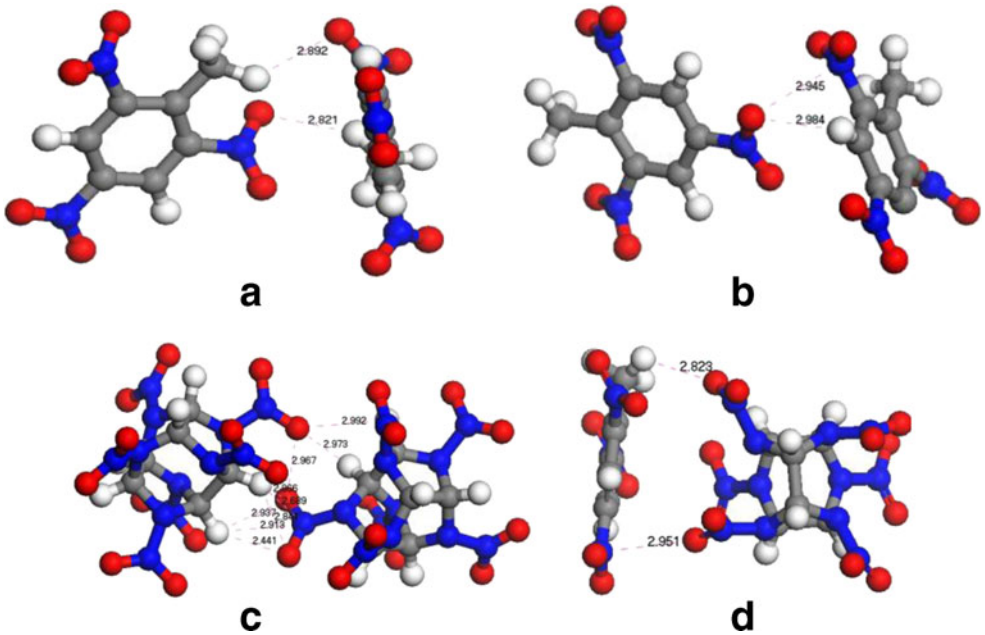

Fig. 2 Atomic interaction lines (AILs) in the intermolecular region between TNT (**a**, **b**) and CL-20 (**c**) dimers in the pure crystal, and TNT/CL-20 dimer (**d**) in the co-crystal

Table 1 Energetic properties of 2,4,6-trinitrotoluene (TNT) molecules and crystals derived by Dmol^3 code. E_C DFT-D correction, E_{TOT} total DFT-D energy, ΔE_{II} intermolecular interaction energy, IT interaction types. ΔE_{II} was obtained by $\Delta E_{II}=E_{TOT}$. **a** and **b** stand for two kinds TNT dimer; **c** and **d** represent 2,4,6,8,10,12-hexanitro-2,4,6,8,10,12-hexaazaisowurtzitane (CL-20) dimer and TNT/CL-20 dimer, respectively

	E_C/(kJ mol^{-1})	E_{TOT}/(kJ mol^{-1})	ΔE_{II}/(kJ mol^{-1})	E_m[a]	IT
TNT	−19.113	/	/	−2,322,232.740	/
CL-20	−55.432	/	/	−4,700,163.537	/
a	−57.541	−4,644,500.136	−34.656	/	TNT_1- C-H…O-N-TNT_2 (2.892) TNT_1- N-O…H-C- TNT_2 (2.821)
b	−47.308	−4,644,485.362	−19.882	/	TNT_1- N-O…N-C- TNT_2 (2.945) TNT_1- N-O…H-C- TNT_2 (2.984)
c	−138.829	−9,400,368.082	−41.008	/	CL-20_1-N-O…(H-C/H-C/O-N)- CL-20_2 CL-20_1-C-H…(O-N/O-N/N-N)- CL-20_2 CL-20_1-C-H…(O-N/O-N/N-N)- CL-20_2
d	−113.977	−7,022,452.666	−56.389	/	CL-20-N-O…N-C- TNT (2.951) CL-20-N-O…H-C- TNT (2.823)

[a] $-\sum E_m$. E_m is the energy of a TNT or a CL-20 molecule

energetic properties of a compound to be predicted successfully at any point r by the nuclei and electrons of a molecule [56, 57].

$$V_{MEP}(r) = \sum_{k}^{nuclei} \frac{Z_k}{|r_k - r|} - \int \psi(r') \frac{1}{|r' - r|} dr' \quad (6)$$

where Z_k is the charge on nucleus k located at r_k. The sign of $Z_k/|r_k - r|$ indicates thus the positive ESP created at any point r by nucleus k, located at r_k. $\int \psi(r') \frac{1}{|r' - r|} dr'$ stands for the negative ESP by electrons at r_k. The sign of $V_{MEP}(r)$ depends on whether the effects of the nuclei or the electrons predominate [58].

The ESPs mapped on the electronic density surface for TNT and CL-20 molecules and supermolecules are given in Fig. 3. We also calculated the ESPs of dimer **a**, **b**, **c** and **d**. It was first demonstrated in a series of papers by Politzer et al. [59–63], and exploited extensively by Rice et al. [64], that the impact sensitivities of explosives are increased by the presence of strongly positive surface potential maxima and by high degrees of internal charge separation. It is notable that the positive ESP on the TNT molecule in TNT/CL-20 dimer is stronger than those of both pure TNT dimers **a** and **b**. The area of positive ESP on the CL-20 molecule in TNT/CL-20 dimer is larger but slightly weaker than that in pure CL-20 dimer **c** and single CL-20 molecule. Moreover, a region of positive ESP exists between the outer surface of TNT and CL-20 in **d**, which obviously involves an intermolecular non-covalent interaction between TNT and CL-20. Thus, the mapped ESP results imply that TNT/CL-20 co-crystal (h_{50}= 99 cm) is less sensitive than CL-20 (h_{50}=47 cm) and more sensitive than TNT (h_{50}>160 cm) by impact [13, 65].

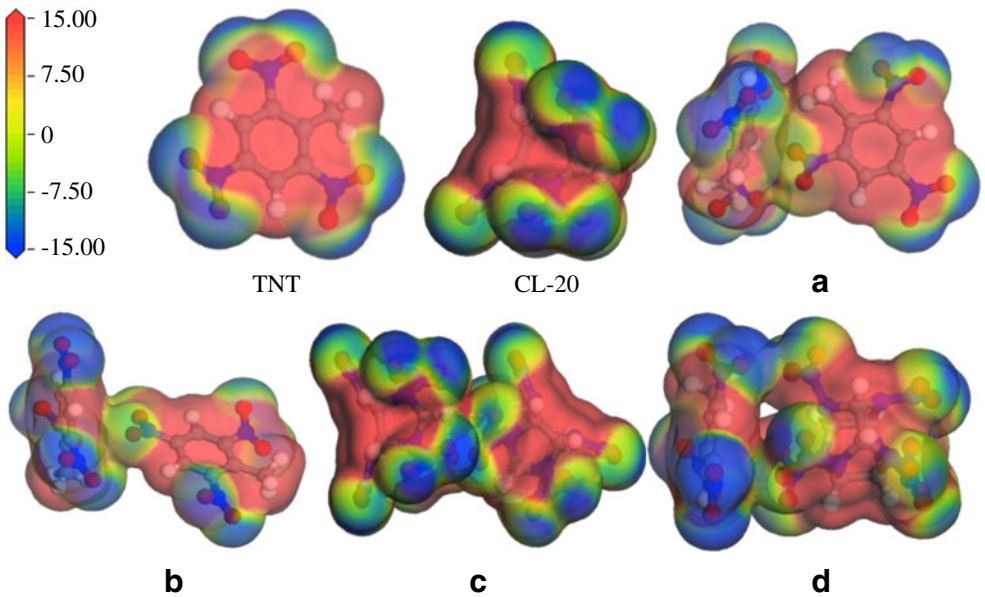

Fig. 3 Electrostatic potential (ESP) surface of TNT, CL-20 and their supermolecules. *Red* and *blue* surfaces represent electron poor and rich regions, respectively, with *colors* representing values between 15.00 kcal mol^{-1} and −15.00 kcal mol^{-1}

Table 2 Summary of the surface electrostatic potential (ESP) of the studied molecules

Molecule	V_{max}/(kJ mol^{-1})	V_{min}/(kJ mol^{-1})	V_{tot}/(kJ mol^{-1})
TNT	186.839	−103.668	83.171
CL-20	279.515	−65.885	213.630
a	222.013	−98.384	123.629
b	196.959	−115.479	81.480
c	290.275	−73.242	217.033
d	254.651	−114.760	139.891

In 2012, Zeman [66] proved that the increase in negative extremes of potentials (V_{min}) and/or the sum (V_{tot}) of V_{min} and positive extremes (V_{max}) correspond to an increase in detonation velocities (D). The data of V_{min}, V_{max} and V_{tot} for the title molecules here are listed in Table 2. It is easy to see that the value of V_{tot} increases in the order **b** < TNT < **a** < **d** < CL-20 < **c**, which indicates that the D of the three compounds increases in the order TNT < TNT/CL-20 co-crystal < CL-20. Finally, it can be deduced that the TNT/CL-20 co-crystal is more powerful than TNT and less sensitive than CL-20.

Additionally, Politzer [58] reported in a very recent review a perspective of "σ-hole" interactions and also stated "π-hole" interactions. The key factors of these two "holes" are both electrostatics/polarization and dispersion. A σ-hole bond is a non-covalent interaction between a covalently bonded atom of Groups IV–VII and a negative site, e.g., a lone pair of a Lewis base or an anion. It was made clear by Politzer [58] that the regions of positive potential can be composed of a series of "σ-holes" or "π-holes". The strengths of the interactions generally correlate well with the magnitudes of the positive and negative ESPs of the σ-hole and the negative site. In our future work, we will pay much more attention to using "σ-holes" or "π-holes" to study non-covalent interactions between energetic molecules.

Intermolecular interaction in crystals

To understand the internal mechanism, the interaction characteristics of different types of regions were shown in scatter graphs (see the above three maps in Fig. 4). The x-axis and y-axis are sign (λ_2) and RDG functions, respectively. A point in the graph corresponds to a grid point.

Figure 4 displays low-gradient isosurfaces (s=0.5 a.u.), subject to the constraint of low density, for TNT/CL-20 co-crystal, CL-20 crystal and TNT crystal. Taking a horizontal line (the blue horizontal line with s=0.5 a.u.), the segments intersected with spikes are just RDG isosurfaces. For each of the three crystals, there are several spikes, and the points in their peaks correspond to critical points in AIM theory. The spikes can be classified into three segments (HBs region, vdWs region and SRs region), ranging from −0.1 to 0.1 a.u. (Fig. 4). In each region, more scatter points reveal greater

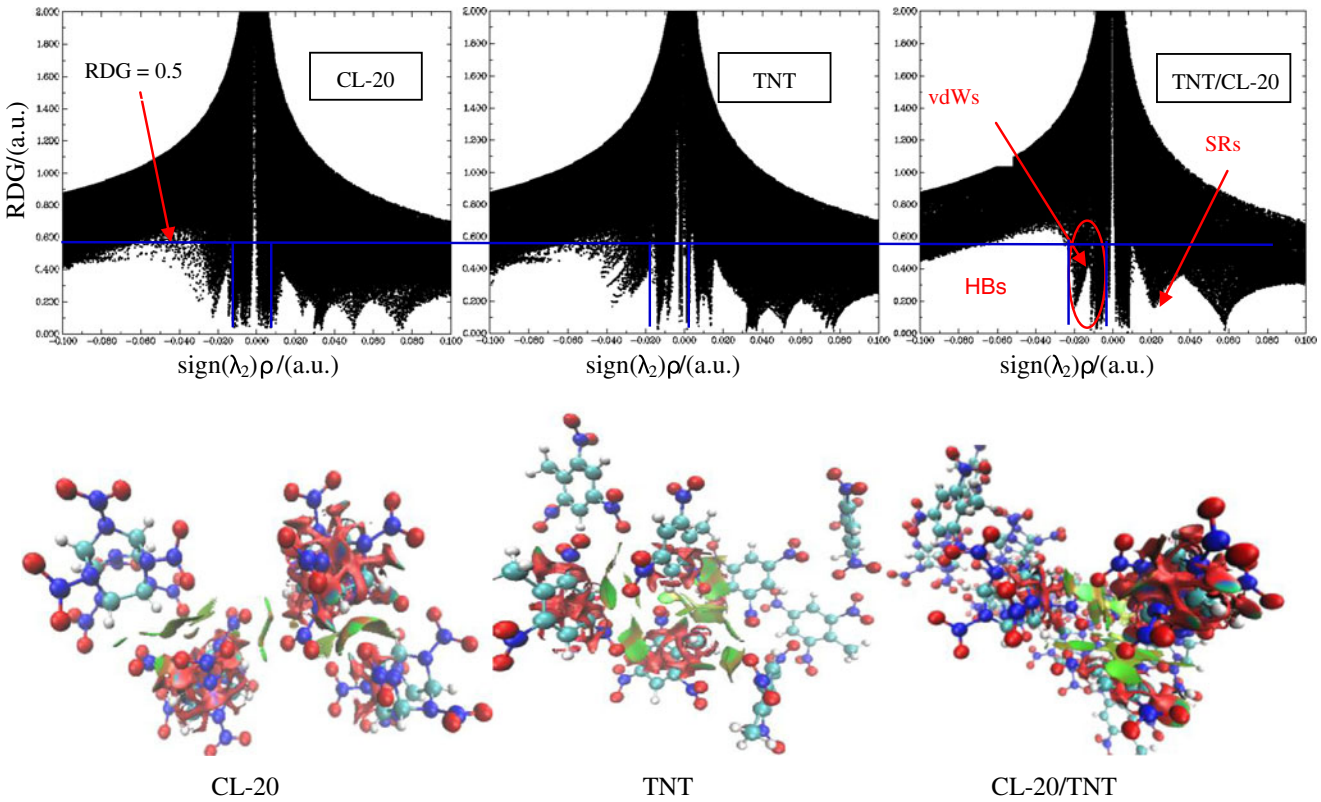

Fig. 4 Gradient isosurfaces (s=0.5 a.u.) for CL-20 crystal, TNT crystal and TNT/CL-20 co-crystal. Peaks appear at $\rho \approx 0.01$ a.u. for vdWs

electron density, that is, greater contribution to total weak interactions. The three interaction regions are divided by two blue vertical lines. It is easy to visualize the lowest electron density between the TNT molecules in TNT crystal among the three compounds. The weak vdWs and HBs combined with the relatively strong SRs result in the brittle property of TNT, which is one of the most important disadvantages or bottlenecks of TNT we need to account for. There are five spikes in the scatter graph of TNT/CL-20 co-crystal, and the points in their peaks are just critical points in AIM theory. The scatter graph of TNT/CL-20 co-crystal contains many more grid points in the vdWs region and fewer grid points in the SRs region, thus implying stronger intermolecular interactions. Thus we can infer that co-crystallization may be a good method to reduce the brittleness of TNT.

Accordingly, from the color-filled RDG isosurfaces, we can identify different type of regions by color (see lower panel of Fig. 4). The surfaces are colored on a blue-green-red scale according to values of sign(λ_2)ρ, ranging from −0.1 to 0.1 a.u. A density cut-off of ρ <0.05 a.u. was chosen since it encapsulates the non-covalent interaction region of interest [24]. Blue indicates strong attractive interactions (HBs), and red indicates strong non-bonded overlap [steric repulsion stacking (SRs) in the center of a molecule]. Furthermore, green indicates weak vdW interactions. A density cut-off of ρ <0.05 a.u. was chosen since it encapsulates the non-covalent interaction region of interest [24].

It is clear that the crystal structure of TNT/CL-20 co-crystal is formed exclusively by interactions involving nitro groups. There are many weak non-covalent interactions propagating through the crystal, and large area of green appear only between TNT and CL-20 molecules. There are no peaks appearing at $\rho \approx 0.05$ a.u., which indicates no strong HBs in TNT/CL-20 co-crystal, although in pure CL-20 crystal the peaks at $\rho \approx 0.04$ a.u. are not very strong. However, it is obvious that the weak vdWs in co-crystal are much stronger than those in pure TNT or CL-20 crystals. There are three kinds of interactions propagating through the crystal: (1) CH hydrogen bonds between oxygen atoms of the nitro group on CL-20 and aliphatic hydrogens of TNT; (2) interactions between the electron-deficient ring of TNT and nitro groups of CL-20, i.e., nitro-aromatic interactions; (3) a series of nitro–nitro interactions between TNT and CL-20, which appears frequently in the co-crystal. We can see easily that there are no strong HBs in the TNT/CL-20 co-crystal. Moreover, it is obvious that the intermolecular electron density of the present three compounds decreases in the order TNT/CL-20 > TNT > CL-20. Finally, we can conclude that it is possible to develop smart energetic materials by "energetic-energetic co-crystals", since this does not necessarily require relatively strong interactions (strong HBs) in co-crystal design.

Mechanical properties

Mechanical properties are of significant importance for energetic materials. The detailed elastic coefficients and effective isotropic mechanical properties of pure TNT, CL-20 and TNT/CL-20 co-crystal in 298 K are listed in Table 3.

From Table 3 it can be seen that some C_{ij} values are much smaller than 10 and the others are much larger than 10, which indicates that the TNT/CL-20 co-crystal has anisotropic behavior to some extent. This anisotropic behavior presumably arises from the crystal packing. It was found that the Young's modulus (E) and Bulk modulus (K) of TNT/CL-20 co-crystal decreased dramatically compared with pure TNT crystal and CL-20 crystal. The modulus decrease means a reduction in rigidity, i.e., the resistance to elastic deformation is decreased. The shear modulus (G) of the co-crystal is slightly smaller than that of CL-20 crystal, but still much larger than that of TNT crystal, which means that there is some reduction in the hardness and tensile strength of the co-crystal. Additionally,

Table 3 Elastic coefficients and effective isotropic mechanical properties of pure TNT, CL-20 and TNT/CL-20 co-crystal

	TNT/CL-20	TNT	CL-20
C_{11}	57.844	61.711	92.277
C_{22}	29.706	39.811	78.698
C_{33}	36.185	47.159	85.022
C_{44}	2.716	14.147	18.895
C_{55}	7.861	4.918	11.449
C_{66}	8.470	19.4185	27.465
C_{12}	23.194	30.173	69.669
C_{13}	43.809	27.045	47.873
C_{14}	2.362	0.193	0.000
C_{15}	13.640	0.109	−10.177
C_{16}	4.786	−0.009	0.000
C_{23}	14.406	40.096	48.841
C_{24}	4.609	−0.025	0.000
C_{25}	2.997	−0.049	−9.605
C_{26}	0.474	−0.011	0.000
C_{34}	9.136	−0.010	0.000
C_{35}	19.374	0.085	2.725
C_{36}	5.705	−0.003	0.000
C_{45}	11.032	−0.002	0.000
C_{46}	−0.346	0.023	1.291
C_{56}	−3.234	−0.005	0.000
λ	28.547	23.905	46.793
μ	6.349	12.828	19.270
Young's modulus (E)	17.891	34.004	52.188
Bulk modulus (K)	25.121	37.514	62.108
Shear modulus (G)	12.044	4.525	12.638
Poisson's ratio (γ)	0.409	0.325	0.354
K/G	4.513	1.868	2.430

the increase in Poisson's ratio (γ) reveals that the co-crystallization of TNT and CL-20 involves an increase in plasticity. Since γ of plastic is usually 0.2–0.4, and it is known that a higher value of *K/G* is associated with malleability and a lower value with brittleness [67], it can, accordingly, be deduced from the values of *K/G* in Table 2 that the TNT/CL-20 co-crystal may have better malleability than its pure components.

Conclusions

Co-crystallization of TNT and CL-20 composes a high-energy and impact-insensitive TNT/CL-20 co-crystal. The results presented here show that hydrogen bonded supramolecular synthons are not indispensable to energetic-energetic co-crystals. The mapped charge densities of local conformation demonstrated that a series of vdWs and stacking interactions maintain the stability of TNT/CL-20 co-crystal. The ESP pictures suggest that TNT/CL-20 co-crystal is more powerful than TNT and less sensitive than CL-20. Three kinds of interactions propagate through the crystal: (1) CH hydrogen bonds between nitro group oxygens on CL-20 and aliphatic hydrogens of TNT; (2) interactions between the electron-deficient ring of TNT and nitro groups of CL-20, i.e., nitro-aromatic interactions; (3) a series of nitro–nitro interactions between TNT and CL-20, which appear frequently in the co-crystal. The scatter graphs also implied that co-crystallization may be a good way to reduce the brittleness of TNT. Calculation of the mechanical properties indicates that the elastic coefficients and effective isotropic mechanical properties of pure TNT, CL-20 crystal can be effectively improved by their co-crystallization. The above results demonstrate the potential to realize more advanced energetic materials by co-crystallization, since most energetic materials contain nitro groups, ring or cage structures, etc.

Acknowledgments The authors are grateful for financial support from National Natural Science Foundation of China—CAEP project (No. 11076002).

References

1. Sikder AK, Sikder N (2004) J Hazard Mater A112:1–15
2. Lara OF, Espinosa PG (2007) Supramol Chem 19:553–557
3. Shan N, Zaworotko MJ (2008) Drug Discov Today 13:440–446
4. Bond DA (2007) Cryst Eng Comm 9:833–834
5. Vishweshwar P, McMahon JA, Bis JA, Zaworotko MJ (2006) Pharm Sci 95:499–516
6. Fried LE, Manaa MR, Pagoria PF, Simpson RLA (2001) Rev Mater Res 31:291–321
7. Agrawal JP, Hodgson RD (2007) Organic chemistry of explosives. Wiley, Chichester
8. Yang ZW, Li HZ, Zhou XQ, Zhang CY, Huang H, Li JS, Nie FD (2012) Cryst Growth Des 12:5155–5158
9. Desiraju GR (1995) Angew Chem Int Ed Engl 34:2311–2327
10. Etter MC (1991) J Phys Chem 95:4601–4610
11. Kira BL, Adam JM (2010) Cryst Growth Des 10:5341–5347
12. Landenberger KB, Matzger AJ (2012) Cryst Growth Des 12:3603–3609
13. Onas B, Adam JM (2011) Angew Chem Int Ed 50:8960–8963
14. Bolton O, Simke LR, Pagoria PF, Matzger AJ (2012) Cryst Growth Des 12:4311–4314
15. Thottempudi V, Shreeve JM (2011) J Am Chem Soc 133:19982–19992
16. Wei CX, Huang H, Duan XH, Pei CH (2011) Propellants Explos Pyrotech 36:416–423
17. Guo CY, Zhang HB, Wang XC, Liu XF, Sun J (2013) J Mater Sci 48: 1351–1357
18. Shen JP, Duan XH, Luo QP (2011) Cryst Growth Des 11:1759–1765
19. Roland B, Dieter B, Georg J (2009) J Am Chem Soc 131:2104–2106
20. Oswald IDH, Motherwell SWD, Parsons SA (2004) Acta Cryst E 60: 1967–1969
21. Basavoju S, Boström D, Velaga PS (2006) Cryst Growth Des 6: 2699–2708
22. Ishweshwar P, McMahon JA, Bis JA, Zaworotko M (2006) J Pharm Sci 95:499–516
23. Hathwar VR, Pal R, Guru Row TN (2010) Cryst Growth Des 10: 3306–3310
24. Erin RJ, Shahar K, Paula MS, Julia CG, Aron JC, Yang WT (2010) J Am Chem Soc 132:6498–6506
25. Liu C, Pilania G, Wang C, Ramprasad R (2012) J Phys Chem A 116: 9347–9352
26. Langreth DC, Lundqvist BI, Chakarova-Käck SD, Cooper VR, Dion M, Hyldgaard P, Kelkkanen A, Kleis J, Kong L, Li S, Moses PG, Murray E, Puzder A, Rydberg H, Schröder E, Thonhauser T (2009) J Phys Condens Matter 21:084203–084217
27. Barone V, Casarin M, Forrer D, Pavone M, Sambi M, Vittadini A (2009) J Comput Chem 30:934–939
28. Dion M, Rydberg H, Schröder E, Langreth DC, Lundqvist BI (2004) Phys Rev Lett 92:246401
29. Ehrlich S, Moellmann J, Reckien W, Bredow T, Grimme S (2011) Chem Phys Chem 12:3414–3420
30. Tkatchenko A, Scheffler M (2009) Phys Rev Lett 102:073005(4)
31. Grimme SJ (2004) Comput Chem 25:1463–1473
32. Grimme SJ (2006) Comput Chem 27:1787–1799
33. Grimme SJ, Antony J, Ehrlich S, Krieg H (2010) J Chem Phys 132: 154104–154123
34. Neumann MA, Perrin MA (2005) J Phys Chem B 109:15531–15541
35. Steven H, Carole AM, Colin RP, Peter JG (2011) Proceedings of the 13th Seminar on New Trends in Research of Energetic Materials, Czech Republic, 245–255
36. Sándor LB, Martin US, Andrew DB (2012) Cryst Eng Comm 14: 1967–1971
37. Bader RFW (1990) Oxford University Press, Oxford (UK)
38. Espinosa E, Souhassou M, Lachekar H, Lecomte C (1999) Acta Cryst B 55:563–572
39. Grabowski SJ (2001) J Phys Chem A 105:10739–10746
40. Hohenberg P, Kohn W (1964) Phys Rev B 136:864–871
41. Becke AD (1995) In: Yarkony DR (ed) Modern electronic structure theory. World Scientific, Singapore, pp 1022–1046
42. Cohen AJ, Mori-Sánchez P, Yang W (2008) Science 321:792–794
43. Zupan A, Burke K, Ernzerhof M, Perdew JP (1997) J Chem Phys 106:10184–10193
44. Julia CG, Erin RJ, Shahar K, Robin C, Piquemal JP, David NB, Yang WT (2011) J Chem Theory Comput 7:625–632
45. Zhang SY, Liu JQ, Yu XX (1992) Beijing Institute of Technology Press, Beijing
46. Theodorou DN, Suter UW (1986) Macromolecules 19:139–154
47. Ma XF, Zhao F, Ji GF, Zhu WH, Xiao JJ, Xiao HM (2008) J Mol Struct (THEOCHEM) 851:22–29

48. Furio E (1997) Spring College in Computational Physics, ICTP, Trieste, June. http://www.fisica.uniud.it/~ercolessi/md/md.pdf
49. Yuji K, Reiko IH, Yoshitaka Y, Shinya M, Atsushi K, Osamu T, Katsuyoshi Y, Kazuyoshi U (2009) J Phys Chem A 113:2551–2560
50. Andersen HC (1980) J Chem Phys 72:2374–2383
51. Allen MP, Tindesley DJ (1989) Oxford University Press, New York
52. Ewald PP (1921) Ann Phys 64:253–287
53. Sun H (1998) J Chem Phys B 102:7338–7364
54. Accelrys Software Inc (2011) Materials studio release notes, release 6.0. Accelrys Software, San Diego
55. Runtz GR, Bader RFW, Messer R (1977) Can J Chem 55:3040–3045
56. Politzer P, Murray JS (2002) Theor Chem Accounts 108:134–142
57. Murray JS, Politzer P (2011) WIREs Comp Mol Sci 1:153–163
58. Politzer P, Murray JS, Clark T (2013) Phys Chem Chem Phys 15: 11178–11189
59. Murray JS, Lane P, Politzer P (1998) Mol Phys 93:187–194
60. Murray JS, Lane P, Politzer P (1995) Mol Phys 85:1–8
61. Politzer P, Murray JS (1995) Mol Phys 86:251–255
62. Murray JS, Lane P, Politzer P (2009) Mol Phys 107:89–97
63. Politzer P, Murray JS (1996) J Mol Struct 376:419–424
64. Rice BM, Hare JJ (2002) J Phys Chem A 106:1770–1783
65. Shu YJ, Huo JC (2011) Chemical Industry Press, Beijing
66. Zeman S, Friedl Z (2012) Propellants Explos Pyrotech 37:609–613
67. Qin L, Xiao HM (2009) J Hazard Mater 164:329–336